Solid Freeform Fabrication 2023: Proceedings of the 34th Annual International Solid Freeform Fabrication Symposium – An Additive Manufacturing Conference
Reviewed Paper

Role of In-situ Monitoring Technique for Digital Twin Development using Direct Energy Deposition: Melt Pool Dynamics and Thermal Distribution

Sung-Heng Wu[1,*], Ranjit Joy[1], Usman Tariq[1], Muhammad Arif Mahmood[2], Frank Liou[1]

[1] Department of Mechanical and Aerospace Engineering, Missouri University of Science and Technology, Rolla, MO 65409, USA.

[2]Intelligent Systems Center, Missouri University of Science and Technology, Rolla, MO 65409, USA.

[*] Corresponding author – Email: swm54@umsystem.edu, Phone: +15734667385, Address: 311 Engineering Research Lab, 500 West 16th Street, Rolla, MO, 65409-0440

Abstract

Direct energy deposition (DED) is a promising additive manufacturing technique that enables the fabrication of complex structures with excellent mechanical properties. The quality of the final product depends on several parameters, including melt pool dynamics and thermal distribution. For process monitoring and continuous improvement of digital twins, in-situ monitoring allows real-time tracking of these parameters, providing valuable data for process optimization. However, existing monitoring methods are limited in their accuracy due to emissivity issues. To address this challenge, an in-house visible spectrum camera has been proposed for real-time process monitoring via dual-wavelength technique. Based on the analyses, the area and thermal distribution inside the melt pool can be estimated accurately. The data from the camera can be integrated into a digital twin's continuous improvement, providing efficiency, and reducing the manufacturing cost.

1 Introduction

Additive manufacturing (AM) has shown significant promise in producing complex shapes, with advantages including enhanced mechanical characteristics, decreased weight, and shortened design times [1]. Among various AM techniques, direct energy deposition (DED) technique has been used by aerospace, healthcare, and offshore industries to manufacture new as well as repair worn-out parts [2]. DED provides huge potential at the verge of difficulties, including quality, dimensions, and reproducibility [3]. Defects such as cracks and keyhole pores can occur even when using pre-optimized process settings due to factors such as localized heat accumulation, surface imperfections, velocity fluctuations, and gas entrapment [4]. The mechanical performance of the printed parts might be severely impacted by the existence of these flaws [5]. To prevent build failures, AM relies heavily on promptly identifying and correcting defects. Ensuring the quality of parts while also saving time and costs simultaneously, the technique of 'in-situ monitoring' is gradually being adopted into AM research[6].

In recent years, there has been a notable surge in research and development activities focused on in-situ monitoring and defect detection in AM [7]. The current cutting-edge in-process sensing technologies employ vision or infrared (IR) thermal sensors to capture essential process characteristics, including melt pool geometries, acoustic emissions, and temperature histories [8]. These sensor outputs are then subjected to post-processing algorithms, such as machine learning (ML) models, to enable defect prediction [9]. Vision-based in-situ monitoring has emerged as a widely adopted method across various AM processes. For instance, real-time surface defect detection can be achieved using vision cameras equipped with ML algorithm [10]. In laser-based AM processes, employing vision sensors with IR optical filters allows for monitoring dynamic behaviors of the molten pool [11]. This information proves valuable in deposition height detection, feedback control, and distinguishing different melting states [12]. Moreover, leveraging additional temperature information, an IR thermal camera demonstrates enhanced effectiveness compared to a visible sensor when observing in-situ dynamics of the melt pool [13]. For instance, an in-situ thermal camera was employed to examine the impact of process parameters and

scan strategies on melt pool characteristics, such as size, shape, powder particle spattering, and heating and cooling rates in laser-based AM [14]. The investigation revealed that dynamic fluctuations in melt pool geometries exhibited associations with microstructure properties. Besides, the thermal diffusvity and layer thickness can also be measured by IR thermographic inspection[15]. Through statistical analysis, crucial temperature features were extracted to identify unstable behaviors in the process plume [16]. A real-time porosity prediction approach was developed, utilizing morphological features extracted from thermal images of the melt pool [17]. ML models were then employed to classify melt pool dynamics and forecast porosity within the manufactured components [18]. Similarly, thermal signatures were linked with convolutional neural networks to capture effects stemming from lack of fusion [19].

The creation and implementation of digital twins (DTs) for laser-based AM processes rely heavily on in-situ monitoring devices [20]. DTs are simulations of real-world systems or processes that can be seen, analyzed, and predicted in real-time [21]. In laser-based AM techniques, DTs can enable process control, optimize process parameters, improve component quality, and provide useful insights into the production process [22]. Data is collected in real-time during the AM process, either from the manufacturing machine or the build environment, and analyzed. In-situ monitoring combined with the DT allows for the collection and application of real-time data. Temperature, melt pool characteristics, powder bed behavior and flow, and laser parameters can all be observed in real-time with the help of in-situ monitoring devices [23]. This information can be fed into the DT to enable real-time monitoring of the process, identification of anomalies, and fine-tuning of the process to achieve maximum efficiency [24]. This aids in the elimination of defects, enhancement of product quality, and the maintenance of stable printing quality. DT can foresee probable flaws by accessing data, including heat gradients, solidification rates, and part geometry [23]. This allows production facilities to detect problems and adjust, reducing waste and efforts. Due to their profound effect on the authenticity and dependability of the DTs, the careful and smart selection of in-situ monitoring device is of utmost importance in the field of DTs [25]. The reliability of the DT model, which depend on the acquired data, rests on the precision and accuracy of the equipment used to gather that data [26]. Careful device selection yields high-quality real-time data, which in turn allows the DT to accurately simulate the dynamics and behavior of its analog [26]. By allowing for comparison and correlation between simulated and real-time data, these monitoring devices are also crucial validators of the DT model. Such intelligent decisions aid in pinpointing areas for model improvement when discrepancies arise, ultimately improving the DT's precision and utility across domains.

In laser-AM, each monitoring device provides specific information, and can only be applied for a particular application. Currently in laser-based AM processes, short-wavelength infrared camera (SWIR) and long wavelength infrared camera (LWIR) and photodiode, are commonly applied to capture thermal distribution in the substrate as well as melt pool and its dynamics during printing process. Table 1 compiles the specifications and limitations of LWIR, SWIR and optical pyrometer. To address all the challenges and limitations posed by in-situ monitoring devices, an in-house visible spectrum camera has been proposed and developed for real-time monitoring using dual-wavelength technique, which can be used for DT improvement effectively.

Table 1. Specifications and limitations of in-situ devices

In-situ device	Wavelength (μm)	Temperature (°K)	Limitations	References
Long wavelength infrared camera	7-14	Measure range 273-1500	• High Temperature measurements • Phase change emissivity issue • High cost	[27]
Short wavelength infrared camera	1-3	Measure range 600-2200	• Can be interfered with laser beam • Phase change emissivity issue • High cost	[27]

Optical Pyrometer	0.3-0.7	Measure range 1000-4000	• Could not detect whole melt pool area; Measuring capacity is limited to 1-16 pixels	[27]

2 Materials and Methods

2.1 Planck's Law and Spectral Radiance

A black body absorbs all radiation and is determined by temperature T. As T increases, the spectral radiance B intensifies, resulting in a shift towards shorter wavelengths, as described by Planck's law. Fig. 1 shows that the correlation of spectral radiance with T having different wavelengths. Charge-coupled devices (CCD) and complementary metal oxide semiconductor (CMOS) always absorb visible wavelengths from 400 to 700 nm. For short-wavelength infrared (SWIR), from 1 to 3 μm, and long-wavelength infrared (LWIR), from 7 to 14 μm, InGaAs and microbolometers are ideally used for designing sensors, respectively[28].

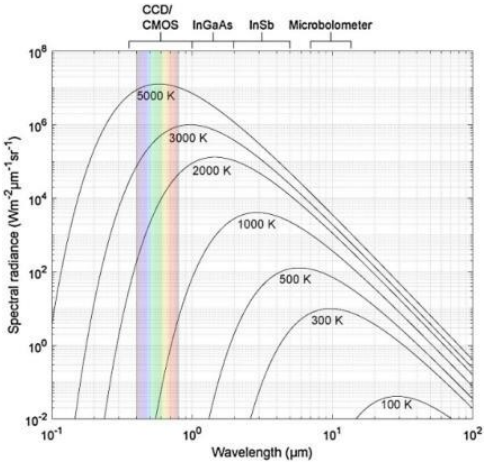

Figure 1. Spectral radiance & wavelength in Planck's law; from Ref [28]

Planck's law has been expressed in Eq. 1 [29] in terms of frequency. However, when calculating the spectral radiance, also known as intensity, emitted from a subject, it is more appropriate to describe Planck's law in terms of wavelength. It is because the material properties of optical sensors are based on their ability to absorb different wavelengths. Planck's law with the wavelength term is described by Eq. 2 [29], where B is the spectral radiance detected by the sensor, λ is the wavelength of the sensor, T is the temperature expressed in Kelvin, h is Planck's constant, c is the speed of light, and K_b is Boltzmann's constant.

Different absorbers are distributed across various wavelength ranges, and each absorber has its suitable temperature measurement range. To determine which devices are appropriate for measurement, obtaining the total spectral radiance can provide the answer. Considering the properties of optical sensors, the spectral radiance absorbed from an object is integration from λ_1 to λ_2, as described in Eq. 3 [29]. Subsequently, conversion from spectral radiance and wavelength to temperature is performed using the inverse Planck law, described in Eq. 4 [29].

$$B_\nu(\nu, T) = \frac{2h\nu^3}{c^2} \frac{1}{e^{\frac{h\nu}{K_B T}} - 1}. \quad (1)$$

$$B_\lambda(\lambda,T) = \frac{2hc^2}{\lambda^5}\frac{1}{e^{\frac{hc}{\lambda K_B T}} - 1}. \quad (2)$$

$$Intensity = \int_{\lambda_1}^{\lambda_2} B(\lambda,T)d\lambda. \quad (3)$$

$$T(\lambda,B) = \int_{\lambda_1}^{\lambda_2} \frac{hc}{K_B}\frac{1}{\lambda \ln\left(\frac{2hc^2}{\lambda^5 B} + 1\right)}. \quad (4)$$

According to the inverse Planck's law, LWIR absorber is capable of measuring temperatures from room temperature to 1500 K. The SWIR absorber, on the other hand, is suitable for measuring high temperatures above 1000 K. Additionally, the visible absorber is effective in detecting high temperatures, particularly for materials with high melting points. Fig. 2(a) illustrates the LWIR is appropriate for measuring low to middle-range temperatures; SWIR and Visible spectrum is proper for middle to high temperature measurements.

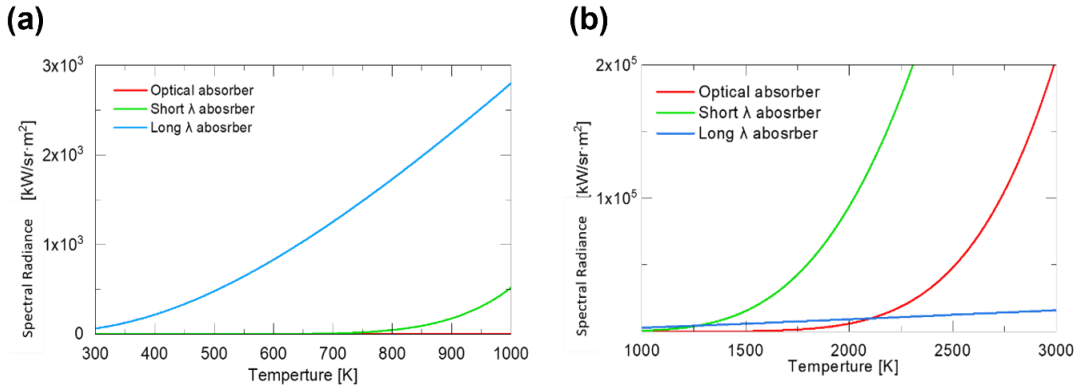

Figure 2. Inverse Planck's law from spectral radiance to temperature **(a)** Low to mid temperature, **(b)** Mid to high temperature

2.2 Dual-Wavelength Method with Visible Spectrum

In the DED process, the commonly used materials, such as Ti6Al4V and high carbon steel, have melting points exceeding 1500 °K. Consequently, SWIR and visible spectral devices are suitable for in-situ monitoring of the melt pool. Considering the interference caused by the laser source, the laser model used in this research is Nd: YAG with a wavelength of 1.067 µm. The visible spectrum presents itself as a potential and reliable candidate for the development of a device to monitor the melt pool. Therefore, a visible spectrum camera equipped with red, green, and blue channels is employed as the measurement device in this research.

The phase change from solid to liquid during the DED process introduces an emissivity issue. In a typical IR camera setup, the emissivity is always constant, leading to inaccurate temperature measurements. However, achieving precise temperature measurements for the melt pool is crucial for the precise training of Digital Twin, especially in the in-situ monitoring stage.

By using the dual wavelength method, as described in Eq. 5[28], the emissivity problem can be solved and an accurate measurement can be attained. With the dual-wavelength method, the object intensity I is detected using two different channels' wavelengths, and the ratio between I_1 and I_2 is determined. Then the ratio is

converted to the corresponding temperature. In Eq. 5, A_1 and A_2 are the combined transmission through different optical devices, such as neutral density (ND) filter, lens, and detectors. The details of combined transmission will be discussed later. ε_1 and ε_2 represent the emissivity for two channels. Since the intensity detected by two channels reaches from the same object and the wavelength between the two channels is close, ε_1 and ε_2 can presumably be eliminated in the Eq. 5 to simplify the calculation.

$$\frac{I_1}{I_2} = \frac{A_1\ \varepsilon_1 {\lambda_2}^5}{A_2\ \varepsilon_2 {\lambda_1}^5} \exp\left(\frac{hc}{K_B T}\left(\frac{1}{\lambda_2} - \frac{1}{\lambda_1}\right)\right). \tag{5}$$

To obtain the T by dual-wavelength method, red and green channels are selected. Since the wavelengths are closer between these two channels, the calculated result from Eq. 5 is more robust. According to Eq.3, it shows that each T will have its corresponding intensity which means that intensity ratio $\frac{I_{Green}}{I_{Red}}$ is also corresponded to T. Hence, T can be derived from the color intensity ratio of red and green signal.

3 Experimental Design

In designing the dual-wavelength visible spectrum device, it is necessary to obtain the intensity of each channel. The sensor used in this design is Sony IMX477, a CMOS type, and the radiance response for sensor is shown in Fig. 3(a). To make the signal imageable, an appropriate lens, Fig. 3(b), is mounted behind the sensor. Considering the deposit position, the lens was selected with focal length = 35mm, aperture = f/2.0, minimum object distance = 200mm and field of view (FOV) = 17.9. After the image and signal is captured by the sensor and lens, saturation is a critical problem that needs to be solved. The laser used in DED process to create melt pool as well as to melt powders is with high intensity; hence, there is a great possibility of saturation, also known as overexposure, on captured signal by each channel. In this scenario, ND filters, reducing the intensity of light uniformly across the spectrum without altering its color or hue, must be placed behind lens to mitigate saturation. Meanwhile, knowing the laser is high energy, placing hot mirror, as shown in Fig. 3(d), behind ND filters can prevent the sensor and lens from being damaged by laser, as shown in Fig. 3(c). The schematic of in-house visible spectrum camera is shown in Fig. 3(e).

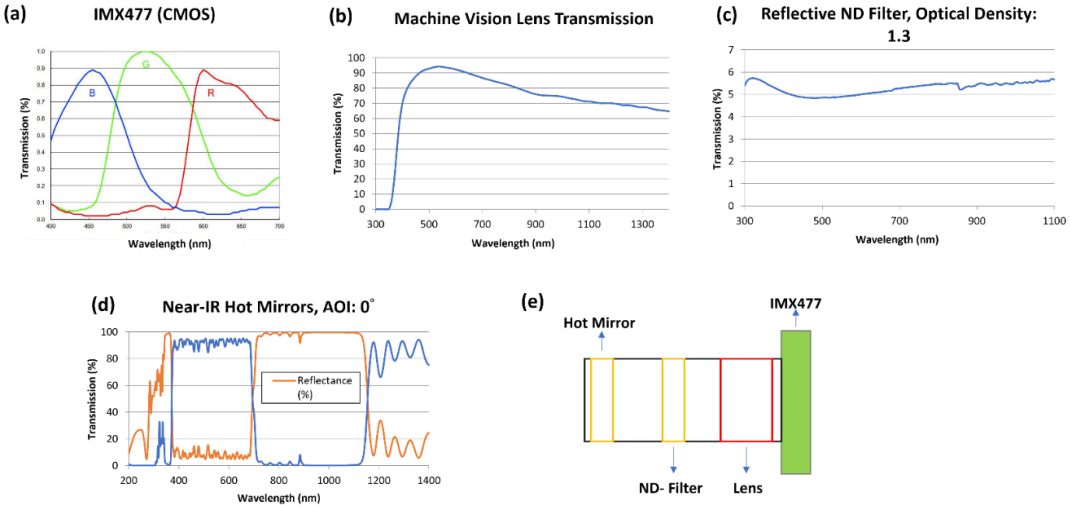

Figure 3. Optical components transmission **(a)** CMOS, **(b)** Lens, **(c)** Reflective ND filter, **(d)** Hot mirror, and **(e)** schematic of visible camera; from Ref. [30] except **(e)**.

In this design, red and green are selected for channel 2 and channel 1, respectively, based on the description Sec. 2.2. In terms of A_1 and A_2, combined transmission, in Eq. 5, the transmission of each optical component must be multiplied since the detected signal is affected by optical components. After calculating intensity with combined transmission, we can obtain the relationship between T and ratio value (I_{Green} / I_{Red}). Fig. 4 shows that the ratio value 0.50294 corresponds to 1700 ˚K, and 0.72497 corresponds to 2400 ˚K.

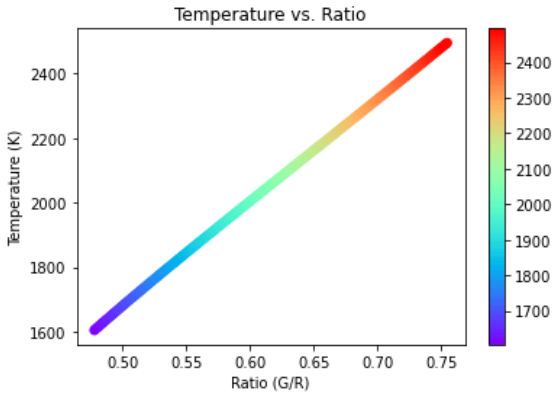

Figure 4. Correlation between temperature and measured intensity ratio(G/R)

Equipment, as shown in Fig. 5, is used in this research having 3-axis table and Nd: YAG laser. SWIR camera is used to monitor the melt pool during glass printing while in-house developed visible camera has been used to monitor the melt pool of high melting point materials such as Ti6Al4V,ceramic, and glass.

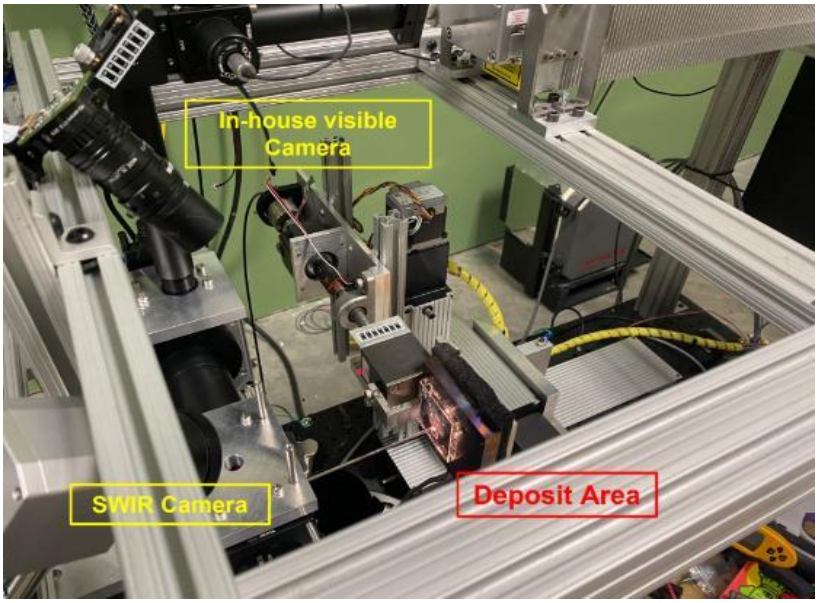

Figure 5. Glass printing DED machine and monitoring equipments setup

4 Results and Discussion

The main objective of this research is to demonstrate the feasibility of using an in-house visible camera with a dual-wavelength method for in-situ monitoring of the melt pool, while also reducing the cost associated with expensive commercial optical equipment. The monitoring results obtained from SWIR, LWIR, and thermocouple

measurements will be presented. Subsequently, this chapter provides a comparison between the in-house camera and a commercial SWIR camera.

The in-house visible camera performs real-time measurements during the DED process. It captures intensity from the red and green channels, calculates the ratio, and then converts it to temperature using Eqs. 3 and 5. Fig. 6 displays the preliminary results of the algorithm based on Planck's law and the dual-wavelength method. The column and row indices represent the coordinates of each pixel. At the coordinates (35, 52), the intensity ratio is 0.561798, which corresponds to a temperature of 1885 °K. In Fig. 6(a), even if some ratios are not zero, they are converted to 0 °K because the measurement range specified in the intensity algorithm is from 1600 to 2500 °K, as shown in Fig. 4. Based on Fig. 2, it is mentioned that a camera with a visible spectrum is more suitable for high-temperature measurements (T > 1800 °K). However, the measurement range is flexible and can be adjusted within the algorithm.

(a) Intensity Ratio ($\frac{I_{Green}}{I_{Red}}$)

	33	34	35	36
45	0	0	0	0
46	0	0	0	0.5
47	0	0	0.483871	0.5375
48	0	0	0.492958	0.529412
49	0	0	0.506667	0.539326
50	0	0.492537	0.531646	0.56383
51	0	0.520548	0.566265	0.57732
52	0.492537	0.551282	0.561798	0.578431

(b) Temperature (°K)

	33	34	35	36
45	0	0	0	0
46	0	0	0	1680
47	0	0	1625	1805
48	0	0	1655	1780
49	0	0	1700	1810
50	0	1655	1785	1890
51	0	1750	1895	1930
52	1655	1850	1885	1935

Figure 6. (a) Intensity ratio and **(b)** converted temperature using dual-wavelength method

During the DED of Ti6Al4V, in-house developed camera can accurately monitor the melt pool area and temperatures pixel by pixel. In Fig. 7(a), the camera analyzes the intensity from the red and green channels for each pixel. The top arrow indicates that the intensity of the red and green channels is 140 and 81, respectively. The bottom arrow indicates that the red and green intensities are 218 and 155, respectively. The trend of the converted temperature is precise because the temperature is higher when the color is closer to white. When the color is white, the intensities of red, blue, and green channels are 255. Conversely, black color corresponds to an intensity of 0 for all three colors. Fig. 7(b) represents a color-mapped graph for a raw image, accurately depicting the thermal distribution of the melt pool. In addition to the in-house camera, LWIR and thermocouple measurements were also used during the deposition process.

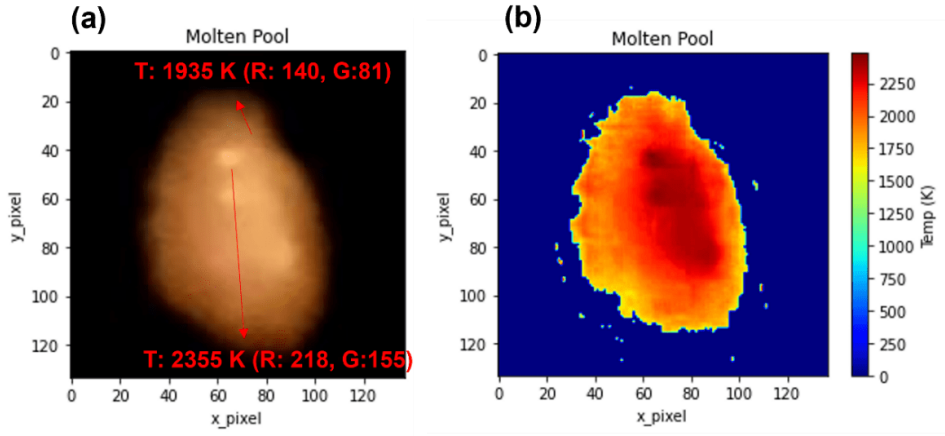

Figure 7. Ti6Al4V deposit melt pool using in-house developed camera **(a)** raw image, and **(b)** post-processed image

Fig. 8 illustrates the limitations of using thermocouple and LWIR devices to monitor the melt pool. Firstly, the LWIR camera is only suitable for measuring temperatures lower than 1800 ºK. Fig. 8(a) shows the deposition schematic while Fig. 8(b) shows the actual deposition and measurement using thermocouple. Fig. 8(c) demonstrates that the LWIR camera can detect low temperatures on the substrate and areas without phase change effectively. However, when it comes to the melt pool, the LWIR camera struggles to distinguish it accurately, resulting in an ambiguous image. Secondly, the thermocouple is unable to withstand the high power from the laser and gets broken during the deposition process, as shown in Fig. 8(b).

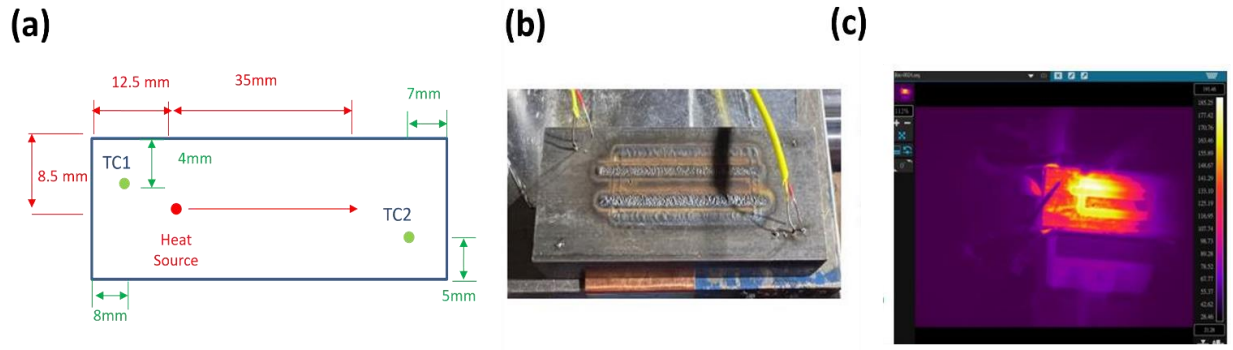

Figure 8. DED deposition **(a)** schematic, **(b)** measurement with thermocouple, and **(c)** long wavelength infrared camera.

To validate the accuracy of in-house visible camera, this research conducted a comparison with commercial SWIR cameras. This comparison was made due to the partial overlap of the SWIR measurement range with the visible spectrum, especially when monitoring high temperatures, as indicated by the results in Fig. 2. During DED of glass, two cameras monitor melt pool simultaneously. The highest melt pool temperatures measured by two cameras agree well, as shown in Fig. 9; in-house visible camera and commercial SWIR measurements are 1655.2 ˚C, and 1636.9 ˚C, respectively. The error between two cameras is 1.1%, proving the feasibility of designing an in-house visible camera. Due to the differences in the mounting positions and the field of view of the two cameras, the raw image displayed on Fig.9(a) may not appear the same as Fig. 9(b). However, despite these variations, the measurement results obtained from both cameras demonstrate a high degree of similarity and exhibit minimal error.

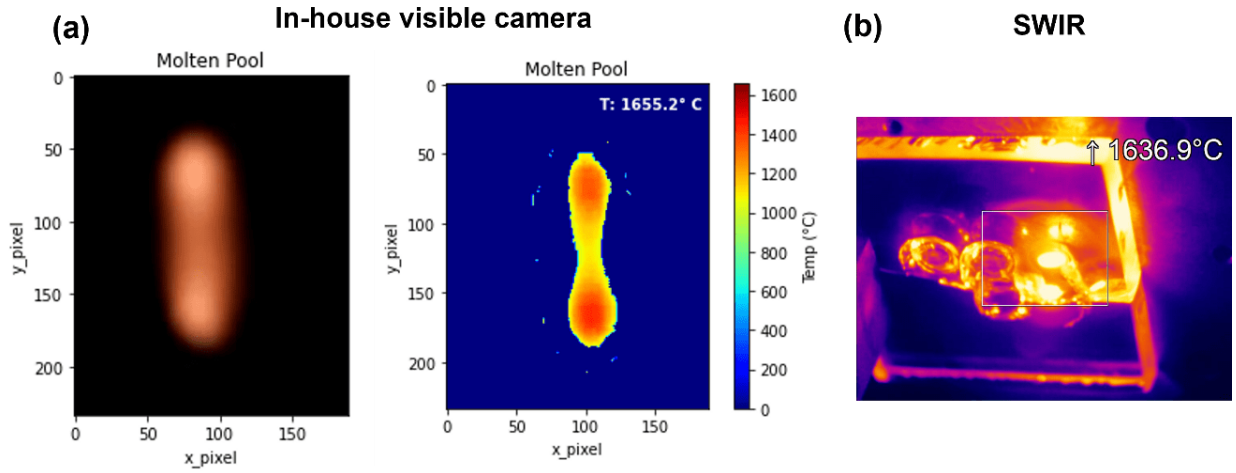

Figure 9. Comparison between **(a)** in-house visible camera and **(b)** commercial short wavelength infrared camera in glass printing using DED.

5 Conclusion

To develop a digital twin of the DED process, in-situ monitoring of the melt pool is crucial because the thermal distribution within the melt pool significantly affects the quality of the deposition. Therefore, it is essential to have an appropriate device for accurate in-situ monitoring of the melt pool, taking into consideration the emissivity issue and the measurement range.

In this research, Planck's law is utilized to assess the measurement range of visible spectrum, SWIR, and LWIR. The results demonstrate that visible and SWIR are reliable for high-temperature measurements. Considering the deposited material with a high melting point and the interference from the laser, a visible spectrum camera proves to be a suitable option. Moreover, the emissivity issue caused by the phase change during the DED process is addressed using a dual-wavelength method. By capturing the intensity radiated by the deposit in two channels, the impact of varying emissivity is eliminated.

The in-house visible camera designed in this research accurately captures the thermal distribution of the melt pool during Ti-6Al-4V deposition. Its accuracy is validated by comparing the measurements with a commercial SWIR camera during glass printing, with an error rate of only 1.1%. Additionally, the cost of the in-house camera design is 20 times lower than that of a commercial camera. These findings demonstrate the feasibility and potential of utilizing a dual-wavelength visible camera for accurate in-situ monitoring, while also reducing instrumentation costs. This research encourages the development of a digital twin for the DED process.

6 Future Work

Based on the aforementioned results, this research defines the role of in-situ monitoring for digital twin development and designs a reliable and cost-effective visible camera for this purpose. The ultimate goal of this series of studies is to develop complete digital twins. The following future work has been proposed:

- Validating the DED process model through experiments and simulations to ensure data reliability.
- Generating low- and high-fidelity data using multi-physics models and experiments to establish a database for machine learning models.
- Designing and constructing an AI surrogate model for predicting melt pool temperature, area, and cooling rate.

Acknowledgement

The support provided by Intelligent Systems Center (ISC) and Dr. Frank Liou at the Missouri University of Science and Technology is appreciated.

References

[1] T. D.Ngo, A.Kashani, G.Imbalzano, K. T. Q.Nguyen, and D.Hui, "Additive manufacturing (3D printing): A review of materials, methods, applications and challenges," *Compos. Part B Eng.*, vol. 143, pp. 172–196, Jun.2018, doi: 10.1016/J.COMPOSITESB.2018.02.012.

[2] D. G.Ahn, "Directed Energy Deposition (DED) Process: State of the Art," *Int. J. Precis. Eng. Manuf. Technol. 2021 82*, vol. 8, no. 2, pp. 703–742, Feb.2021, doi: 10.1007/S40684-020-00302-7.

[3] M. A.Mahmood *et al.*, “Bridging the analytical and artificial neural network models for keyhole formation with experimental verification in laser melting deposition: A novel approach,” *Results Phys.*, vol. 26, p. 104440, Jul.2021, doi: 10.1016/J.RINP.2021.104440.
[4] D.Svetlizky *et al.*, “Directed energy deposition (DED) additive manufacturing: Physical characteristics, defects, challenges and applications,” *Mater. Today*, vol. 49, pp. 271–295, Oct.2021, doi: 10.1016/J.MATTOD.2021.03.020.
[5] J. M.Wilson, C.Piya, Y. C.Shin, F.Zhao, and K.Ramani, “Remanufacturing of turbine blades by laser direct deposition with its energy and environmental impact analysis,” *J. Clean. Prod.*, vol. 80, pp. 170–178, Oct.2014, doi: 10.1016/J.JCLEPRO.2014.05.084.
[6] U.Tariq, R.Joy, S. H.Wu, M. A.Mahmood, A. W.Malik, and F.Liou, “A state-of-the-art digital factory integrating digital twin for laser additive and subtractive manufacturing processes,” *Rapid Prototyp. J.*, no. August, 2023, doi: 10.1108/RPJ-03-2023-0113.
[7] M.Arif Mahmood, F.Ghassan Alabtah, Y.AlHamidi, and M.Khraisheh, “On the laser additive manufacturing of high-entropy alloys: A critical assessment of in-situ monitoring techniques and their suitability,” *Mater. Des.*, vol. 226, p. 111658, Feb.2023, doi: 10.1016/J.MATDES.2023.111658.
[8] L.Kong, X.Peng, Y.Chen, P.Wang, and M.Xu, “Multi-sensor measurement and data fusion technology for manufacturing process monitoring: a literature review,” *Int. J. Extrem. Manuf.*, vol. 2, no. 2, p. 022001, Mar.2020, doi: 10.1088/2631-7990/AB7AE6.
[9] J.Qin *et al.*, “Research and application of machine learning for additive manufacturing,” *Addit. Manuf.*, vol. 52, p. 102691, Apr.2022, doi: 10.1016/J.ADDMA.2022.102691.
[10] H.Baumgartl, J.Tomas, R.Buettner, and M.Merkel, “A deep learning-based model for defect detection in laser-powder bed fusion using in-situ thermographic monitoring,” *Prog. Addit. Manuf.*, vol. 5, no. 3, pp. 277–285, Sep.2020, doi: 10.1007/S40964-019-00108-3/FIGURES/4.
[11] L.Mazzoleni, A. G.Demir, L.Caprio, M.Pacher, and B.Previtali, “Real-Time Observation of Melt Pool in Selective Laser Melting: Spatial, Temporal, and Wavelength Resolution Criteria,” *IEEE Trans. Instrum. Meas.*, vol. 69, no. 4, pp. 1179–1190, Apr.2020, doi: 10.1109/TIM.2019.2912236.
[12] B.Chen, Y.Yao, C.Tan, Y.Huang, and J.Feng, “A study on spectral characterization and quality detection of direct metal deposition process based on spectral diagnosis,” *Int. J. Adv. Manuf. Technol.*, vol. 96, no. 9–12, pp. 4231–4241, Jun.2018, doi: 10.1007/S00170-018-1889-X/METRICS.
[13] M.Khanzadeh, S.Chowdhury, M. A.Tschopp, H. R.Doude, M.Marufuzzaman, and L.Bian, “In-situ monitoring of melt pool images for porosity prediction in directed energy deposition processes,” *https://doi.org/10.1080/24725854.2017.1417656*, vol. 51, no. 5, pp. 437–455, May2018, doi: 10.1080/24725854.2017.1417656.
[14] M.Yakout, I.Phillips, M. A.Elbestawi, and Q.Fang, “In-situ monitoring and detection of spatter agglomeration and delamination during laser-based powder bed fusion of Invar 36,” *Opt. Laser Technol.*, vol. 136, p. 106741, Apr.2021, doi: 10.1016/J.OPTLASTEC.2020.106741.
[15] T.Liu, E. C.Kinzel, and M. C.Leu, “In-situ lock-in thermographic measurement of powder layer thermal diffusivity and thickness in laser powder bed fusion,” *Addit. Manuf.*, vol. 74, no. August, p. 103726, 2023, doi: 10.1016/j.addma.2023.103726.
[16] M.Grasso, A. G.Demir, B.Previtali, and B. M.Colosimo, “In situ monitoring of selective laser melting of zinc powder via infrared imaging of the process plume,” *Robot. Comput. Integr. Manuf.*, vol. 49, pp. 229–239, Feb.2018, doi: 10.1016/J.RCIM.2017.07.001.
[17] M.Khanzadeh, S.Chowdhury, M.Marufuzzaman, M. A.Tschopp, and L.Bian, “Porosity prediction: Supervised-learning of thermal history for direct laser deposition,” *J. Manuf. Syst.*, vol. 47, pp. 69–82, Apr.2018, doi: 10.1016/J.JMSY.2018.04.001.
[18] P.Akbari *et al.*, “MeltpoolNet: Melt pool characteristic prediction in Metal Additive Manufacturing using machine learning,” *Addit. Manuf.*, vol. 55, p. 102817, Jul.2022, doi: 10.1016/J.ADDMA.2022.102817.

[19] A.Karthikeyan, H.Balhara, A. K.Lianos, A.Hanchate, and S. T. S.Bukkapatnam, “In-situ surface porosity prediction in DED (directed energy deposition) printed SS316L parts using multimodal sensor fusion,” Apr.2023.
[20] Y.Lu, E.Shevtshenko, and Y.Wang, “Physics-based compressive sensing to enable digital twins of additive manufacturing processes,” *J. Comput. Inf. Sci. Eng.*, vol. 21, no. 3, Jun.2021, doi: 10.1115/1.4050377/1102045.
[21] F.Tao, Q.Qi, L.Wang, and A. Y. C.Nee, “Digital Twins and Cyber–Physical Systems toward Smart Manufacturing and Industry 4.0: Correlation and Comparison,” *Engineering*, vol. 5, no. 4, pp. 653–661, Aug.2019, doi: 10.1016/J.ENG.2019.01.014.
[22] F.He *et al.*, “Research and application of artificial intelligence techniques for wire arc additive manufacturing: a state-of-the-art review,” *Robot. Comput. Integr. Manuf.*, vol. 82, p. 102525, Aug.2023, doi: 10.1016/J.RCIM.2023.102525.
[23] S.Clijsters, T.Craeghs, S.Buls, K.Kempen, and J. P.Kruth, “In situ quality control of the selective laser melting process using a high-speed, real-time melt pool monitoring system,” *Int. J. Adv. Manuf. Technol.*, vol. 75, no. 5–8, pp. 1089–1101, Oct.2014, doi: 10.1007/s00170-014-6214-8.
[24] P.Eirinakis *et al.*, “Enhancing Cognition for Digital Twins,” *Proc. - 2020 IEEE Int. Conf. Eng. Technol. Innov. ICE/ITMC 2020*, Jun.2020, doi: 10.1109/ICE/ITMC49519.2020.9198492.
[25] K.Bartsch, A.Pettke, A.Höbert, J.Lakämper, and F.Lange, “On the digital twin application and the role of artificial intelligence in additive manufacturing: a systematic review,” *J. Phys. Mater.*, vol. 4, no. 3, p. 032005, Apr.2021, doi: 10.1088/2515-7639/ABF3CF.
[26] M.Pantelidakis, K.Mykoniatis, J.Liu, and G.Harris, “A digital twin ecosystem for additive manufacturing using a real-time development platform,” *Int. J. Adv. Manuf. Technol.*, vol. 120, no. 9–10, pp. 6547–6563, Jun.2022, doi: 10.1007/S00170-022-09164-6/FIGURES/15.
[27] “Non-Visible Imaging: Thermal Cameras & Long-Wave Infrared (LWIR).”
[28] P. A.Hooper, “Melt pool temperature and cooling rates in laser powder bed fusion,” *Addit. Manuf.*, vol. 22, pp. 548–559, Aug.2018, doi: 10.1016/j.addma.2018.05.032.
[29] “Planck’s law.” https://en.wikipedia.org/wiki/Planck%27s_law
[30] “THORLABS.” https://www.thorlabs.com/newgrouppage9.cfm?objectgroup_id=897